Proceedings of BS2013:
13th Conference of International Building Performance Simulation Association, Chambéry, France, August 26-28

EFFICIENCY AND ACCURACY OF DIFFERENT POTENTIALS FOR THE SIMULATION OF MOISTURE TRANSFER IN BUILDING MATERIALS

Hans Janssen[1]
[1]Building Physics Section, Department of Civil Engineering, KU Leuven,
Kasteelpark Arenberg 40, 3001 Leuven, Belgium

ABSTRACT

Much disparity exists on the numerical efficiency and accuracy of different potentials for moisture transfer in building materials, with various implicit claims but no actual corroboration. This paper aims at providing such evidence by comparing the numerical efficiency and accuracy of capillary pressure, relative humidity and -log(-capillary pressure) for a suite of benchmark simulations. The study shows that capillary pressure and relative humidity outperform -log(-capillary pressure), as the latter is plagued by its highly non-linear moisture capacity near saturation. Capillary pressure and relative humidity are thus the potentials of choice.

INTRODUCTION

Moisture transfer in building materials plays a critical role in the durability and sustainability of built structures, and in the health and comfort of building occupants. Two selected illustrations are the corrosion of rebars in concrete due to chloride ingress via the pore water, and the formation of mould on interior finishes owing to excessive interior humidity levels. Numbers from the United States indicate that the proportion of current US asthma cases attributable to dampness and mould exposure is just over 20 % (Mudarri and Fisk, 2007), and that roughly one out of four US bridges is structurally deficient, often as the result of reinforcement corrosion (AASHO, 2008). The reliable assessment of moisture transfer in building materials is thus crucial, requiring efficient numerical tools for unsaturated moisture transfer in porous building materials.

Numerical simulation of moisture transfer in building materials has taken a high flight in the last few decades, and is becoming progressively more common in engineering research and practice. Several simulation packages are now available to practitioners (Delphin, WUFI, …), and many more are being applied by researchers. Delgado et al. (2013) report on more than 50 tools for hygrothermal simulation of building materials and building components, Woloszyn and Rode (2008) describe more than 15 tools for hygrothermal simulation of whole buildings. Numerical simulation of moisture and heat transfer has recently undergone standardisation (EN 15026, 2007), and a complementary quality assessment methodology is also available (Hagentoft et al., 2004). Notwithstanding these unification efforts though, much disparity still exists on which moisture potential is best applied in numerical simulations of moisture transfer in building materials.

In heat transfer, 'temperature' is commonly accepted as the governing potential, and all simulation packages hence use temperatures as the unknown variables to solve. In soil physics 'matric head' – closely related to capillary pressure – is also widely recognised as governing potential and unknown variable for simulations of unsaturated soil moisture transfer. For moisture transfer in building materials, such unified state has not been accomplished yet: models apply capillary pressure (Janssen et al., 2007), relative humidity (Tariku et al., 2010), water vapour fraction (Steeman et al., 2009), water vapour content (Qin et al., 2009), water vapour pressure (Janssens, 2001), volumetric moisture content (Mendes et al., 2002), water chemical potential (Matsumoto and Tanaka, 1991), log of capillary pressure (Pedersen, 1992). The given references should be considered as mere examples, more cases in point can be found in (Delgado et al., 2013).

In most cases, no clear arguments are put forward for the choice for a particular moisture potential. In earlier days, much of this disparity on moisture potential possibly stemmed from variations in the physical description of moisture transfer: different authors introduced differing models for moisture transfer, based on different moisture transfer potentials, which were then maintained in the numerical implementation. It has now been firmly established though that capillary pressure and vapour pressure are the governing transfer potentials for liquid and vapour respectively (Funk and Wakili, 2008; Janssen, 2011). In recent days, the moisture potential disparity is probably mainly related to opinions on numerical efficiency and/or accuracy: a particular potential is assumed to dampen the non-linearity of the moisture transfer equation, a specific potential is preferred since it operates within a more limited range, ... amid other arguments. At this point in time though, no support for these – often implicit – efficiency and accuracy claims is available in literature. This article hence aims at providing such corroboration, to allow a more rational moisture potential choice in current and future models and tools.

This paper is hence built up as follows. In the subsequent sections the numerical model and four benchmark simulations are put forward. These benchmarks are then performed with different moisture potentials, and their relative efficiency and accuracy are assessed via their numbers of required iterations and their deviations from a reference solution. The principal observations from that assessment are presented next, to lastly bring the paper to an end with the conclusions. These will allow a more rational choice of the optimal moisture potential for the efficient and accurate simulation of moisture transfer in building materials, and thus contribute to the reliable assessment of moisture transfer in building materials.

2. NUMERICAL MODEL

2.1 Moisture transfer

As the efficiency and accuracy claims mainly refer to the numerical difficulty of the moisture transfer equation, all benchmark simulations are about isothermal moisture transfer. The basic physical model for isothermal moisture transfer can be described as:

$$\frac{\partial w}{\partial t} = -\nabla(g_l + g_v) = \nabla(k_l \nabla p_c + \delta_v \nabla p_v) \qquad (1)$$

with w [kg/m] volumetric moisture content, g_l and g_v [kg/m s] liquid and vapour flux, p_c and p_v [Pa] capillary and vapour pressure, k_l and δ_v [kg/msPa] liquid and vapour permeability, and t [s] time. In this study, three potentials are examined: capillary pressure p_c, relative humidity φ [-], and -$\log_{10}$(-capillary pressure) lp_c [$\log_{10}$(Pa)]. In isothermal conditions, relative humidity is proportional to water vapour pressure/fraction/content, and the capillary pressure is equivalent to water chemical potential, hence bringing the actual number of analysed potentials to seven. Volumetric moisture content is not studied here, as it is not a true continuous potential. Equation 1 thus transforms into three versions, for respectively p_c, φ, lp_c:

$$\frac{\partial w}{\partial p_c}\frac{\partial p_c}{\partial t} = \nabla\left(\left(k_l + \delta_v p_{v,sat}\frac{\partial \varphi}{\partial p_c}\right)\nabla p_c\right) \qquad (2a)$$

$$\frac{\partial w}{\partial p_c}\frac{\partial p_c}{\partial \varphi}\frac{\partial \varphi}{\partial t} = \nabla\left(\left(k_l \frac{\partial p_c}{\partial \varphi} + \delta_v p_{v,sat}\right)\nabla \varphi\right) \qquad (2b)$$

$$-p_c ln(10)\frac{\partial w}{\partial p_c}\frac{\partial lp_c}{\partial t} = \nabla\left(-p_c ln(10)\left(k_l + \delta_v p_{v,sat}\frac{\partial \varphi}{\partial p_c}\right)\nabla lp_c\right) \qquad (2c)$$

with $p_{v,sat}$ [Pa] is the saturation vapour pressure, and wherein the derivatives from p_c to φ or vice versa can be derived from Kelvin's law. In general Equations 2a-c can be presented as:

$$c\frac{\partial U}{\partial t} - \nabla(k\nabla U) = 0 \qquad (3)$$

with U, c, k the moisture potential, moisture capacity and moisture permeability respectively.

2.2 Numerical solution

The moisture transfer equation in Equation 3 is solved numerically by application of a finite-element spatial discretisation and backward-Euler temporal discretisation, in combination with a mass-conservative iterative method (Janssen et al., 2007) and adaptive numerical integration for the element matrices (Janssen, 2010). This converts Equation (3) into a system of algebraic equations:

$$(\boldsymbol{C}^{t+\Delta t,i} + \Delta t\boldsymbol{K}^{t+\Delta t,i})\boldsymbol{U}^{t+\Delta t,i+1} = \Delta t\boldsymbol{F}^{t+\Delta t,i} + \boldsymbol{C}^{t+\Delta t,i}U^{t+\Delta t,i} + \boldsymbol{S}^{t+\Delta t,i} - \boldsymbol{S}^{t} \qquad (4)$$

with **C** and **K** the capacity and permeability matrices, **U**, **F** and **S** the potential, load and saturation vectors, Δt [s] the time step, and i the iteration number. The resulting system of equations is linearised through the Picard and Newton-Raphson iterative scheme for respectively material properties and boundary conditions, and finally solved by standard R^TR Cholesky decomposition and backsubstitution.

The algorithm uses a two-pronged convergence criterion for the iterative process, evaluating residuals of moisture potentials and moisture contents:

$$min\left(\begin{matrix}\frac{\|\boldsymbol{U}^{t+\Delta t,i+1} - \boldsymbol{U}^{t+\Delta t,i}\|}{\|\boldsymbol{U}^{t+\Delta t,i+1}\|} \\ \frac{\|\boldsymbol{W}^{t+\Delta t,i+1} - \boldsymbol{W}^{t+\Delta t,i}\|}{\|\boldsymbol{W}^{t+\Delta t,i+1}\|}\end{matrix}\right) \leq 10^{-6} \qquad (5)$$

with **W** the moisture content vector. Such global criterion is preferred, to avoid a strong effect of incidental local numerical deviations. The algorithm moreover applies a heuristic time-step adaptation scheme based on the number of iterations that were required to obtain convergence in the previous time step:

$$\Delta t_{j+1} = \Delta t_j min\left(max\left(\frac{i_{max}}{2i_j}, 0.5\right), 2\right) \qquad (6)$$

with Δt_j and Δt_{j+1} [s] the previous and next time step, i_j the number of iterations for time step Δt_j, and i_{max} the maximum number of permitted iterations (30 in this investigation). Additional implementations to tackle output moments and divergent steps are also in place. More info on the specific numerical methods can be found in (Janssen et al., 2007; Janssen, 2010).

3. BENCHMARK SIMULATIONS

3.1 Benchmark simulations

Four benchmark simulations are selected: hygroscopic adsorption, driving rain, isothermal drying, capillary absorption. These cases are all typical examples of moisture transfer in building materials, and they represent a broad range of moisture transfer occurrences. They are simulated with two different materials: ceramic brick and cement mortar. The ceramic brick is an example of a non-hygroscopic but fairly permeable material while the cement mortar is more hygroscopic but less permeable. This way, a wide range of possible materials is represented.

For hygroscopic adsorption, driving rain, isothermal drying and capillary absorption respectively, the initial and boundary conditions are:

$$t < 0\ s\ \&\ x \in [0.0; 0.1]: \quad \varphi = 0.5$$
$$t \geq 0\ s\ \&\ x = 0.0\ m: \quad g_{v,s} = 10^{-7} \cdot p_{v,sat} \cdot (0.97 - \varphi_s)\ kg/m^2 s \tag{7}$$

$$t < 0\ s\ \&\ x \in [0.0; 0.1]: \quad \varphi = 0.5$$
$$t \geq 0\ s\ \&\ x = 0.0\ m: \quad g_{l,s} = 2 \cdot 10^{-5}\ kg/m^2 s \tag{8}$$

$$t < 0\ s\ \&\ x \in [0.0; 0.1]: \quad p_c = -10^3\ Pa$$
$$t \geq 0\ s\ \&\ x = 0.0\ m: \quad g_{v,s} = 10^{-7} \cdot p_{v,sat} \cdot (0.5 - \varphi_s)\ kg/m^2 s \tag{9}$$

$$t < 0\ s\ \&\ x \in [0.0; 0.1]: \quad \varphi = 0.5$$
$$t \geq 0\ s\ \&\ x = 0.0\ m: \quad p_{c,s} = -10^3\ Pa \tag{10}$$

with x [m] the coordinate and subscript s [-] referring to the surface value. In every benchmark, the other boundary is considered impermeable, and all simulations are performed at 20 °C. For ceramic brick and cement mortar respectively, the hygroscopic adsorption is simulated for $5 \cdot 10^5$ and $1 \cdot 10^7$ s, driving rain for $1 \cdot 10^5$ and $1 \cdot 10^5$ s, isothermal drying for $1 \cdot 10^6$ and $5 \cdot 10^7$ s, and capillary absorption for $5 \cdot 10^3$ and $2.5 \cdot 10^4$ s. Alphanumeric output is requested at every 2 % of the total simulation time, and every simulation starts with a suitable initial time step. Material properties for the ceramic brick and cement mortar are illustrated in Figure 1.

3.2 Spatial discretisations

The benchmark simulations are performed with different spatial discretisations. For all cases concerned, the moisture potential profiles become progressively smoother deeper in the material, implying that a coarsening discretisation is more appropriate than an equidistant one. All the discretisations are developed based on a 'grid factor' A, which determines the first internode distance and the internode distance growth factor. Increasing A will thus result in a coarser spatial discretisation. Concretely, all discretisations are developed based on discrete values for A, taken from the [100;1000] interval:

$$\Delta x_1 = 10^{-6} \cdot A$$
$$\Delta x_{j+1} = min\left[\Delta x_j \cdot (1 + 10^{-3} \cdot A), 0.01\right] \tag{11}$$

with Δx_j the internode distance between node j and j + 1. For example, for A 100, Δx_1 is $1 \cdot 10^{-4}$ m, Δx_2 is 1. $1 \cdot 10^{-4}$ m, …. The finest grid consists of 49 nodes, the roughest of 13 nodes. All discretisations apply quadratic line elements, with 3 nodes per element.

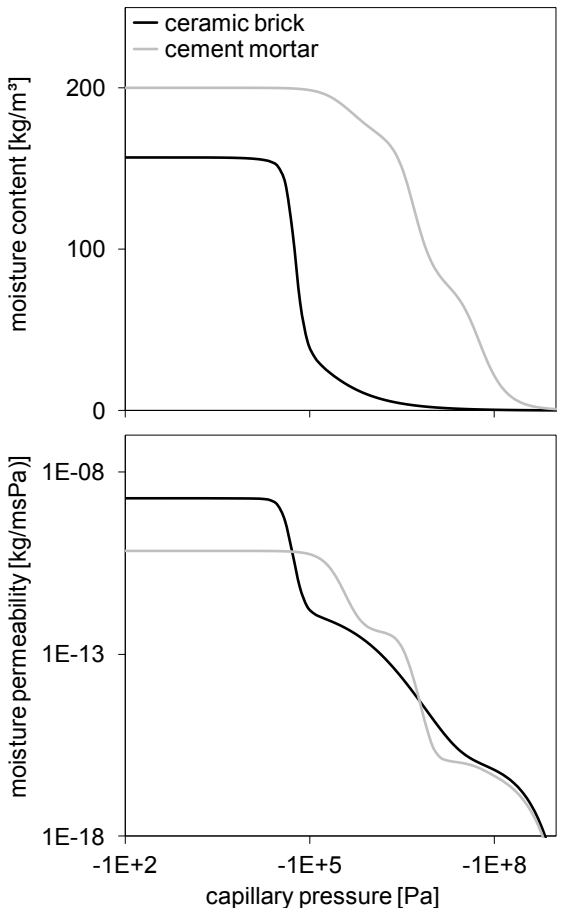

Figure 1: Moisture retention curve (top) and total moisture permeability (bottom) for ceramic brick and cement mortar; the right-hand side of Equation (2.a) defines the total permeability.

3.3 Performance criteria

The numerical efficiency of the various moisture potentials is evaluated by comparison of the total number of iterations required for the complete simulation. These, in combination with the number of operations necessary for matrix composition and decomposition per iteration determine the computational cost of the simulation, and can thus be used to judge the numerical efficiency. The assessment however also needs to take the numerical accuracy of the simulation results into consideration, as efficient but inaccurate simulations are unwanted. The numerical accuracy is evaluated by comparing the results from the simulations to reference solutions obtained with a fine temporal and spatial discretisation. Here the mass error E – average relative deviation from the reference mass evolution – is used (Janssen, 2010):

$$E = \sqrt{\sum_{j=1}^{n} \left(\frac{m_j - m_{j,ref}}{m_{j,ref}} \right)^2 / n} \tag{12}$$

with $m_{j(,ref)}$ the total moisture masses in the actual and reference solution at output moment j, and n the total number of output moments (50 in this study).

4. PRESENTATION OF RESULTS

The entire study comprises 2 materials, 3 potentials, 4 benchmarks and 12 discretisations (eleven standard and one reference), amounting to 288 simulations to be reported. The results put forward here are the required numbers of iterations to complete the entire simulation interval and the mass errors E indicating the deviations from the reference solution. The four considered benchmarks – hygroscopic adsorption, driving rain, isothermal drying, capillary absorption – are depicted in respectively Figures 2, 3,4 and 5.

For each combination of benchmark and material, the reference solution is obtained by averaging the reference discretisation outcomes for the three potentials. In almost all instances, the internal deviation between these three reference discretisation outcomes is (far) smaller than the mass errors E observed for the standard discretisations, hence confirming the accuracy of the reference solutions. Only for the 'driving rain & cement mortar' combi, the reference solution's accuracy hovers around 10^{-4}, which is thus close to the mass errors obtained for 'capillary pressure'.

In all graphs, the results for ceramic brick are shown at the top, those for cement mortar at the bottom. The full markers relate to the number of iterations (on left axis), the hollow markers to the mass errors (on right axis). One should moreover be aware that in many graphs the vertical axes are scaled differently, and that the 0-level of the left axis has been raised somewhat to lessen overlaps between full and hollow markers.

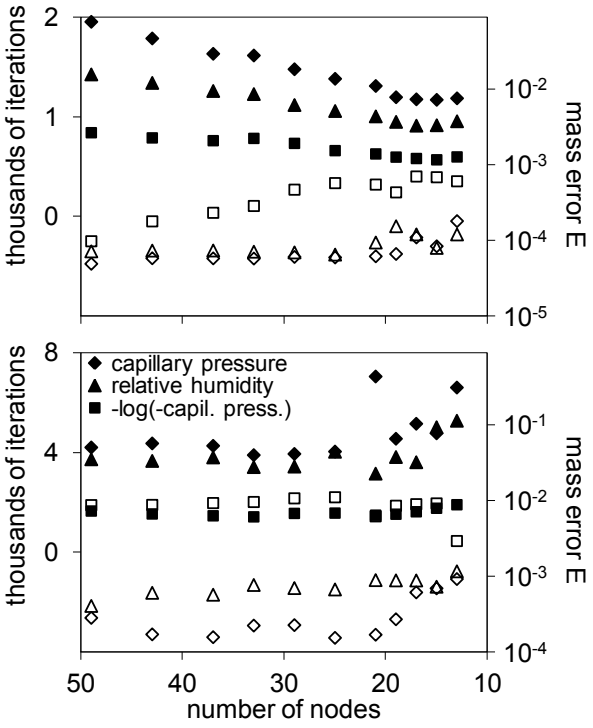

Figure 3: number of needed iterations and resulting mass errors for 'driving rain' for ceramic brick (top) and cement mortar (bottom). Full markers represent the numbers of iterations (left axis), hollow markers stand for the mass errors (right axis).

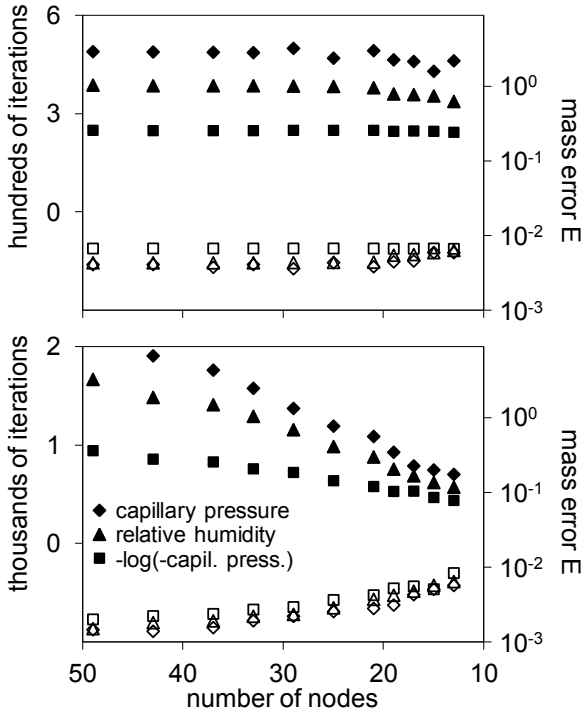

Figure 2: numbers of needed iterations and resulting mass errors for 'hygroscopic adsorption' for ceramic brick (top) and cement mortar (bottom). Full markers represent the numbers of iterations (left axis), hollow markers stand for the mass errors (right axis).

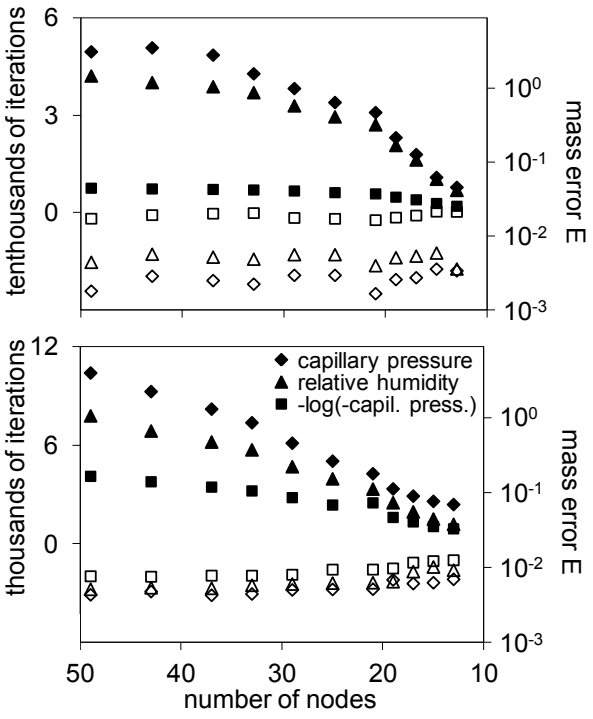

Figure 4: number of needed iterations and resulting mass errors for 'isothermal drying' for ceramic brick (top) and cement mortar (bottom). Full markers stand for the numbers of iterations (left axis), hollow markers represent the mass errors (right axis).

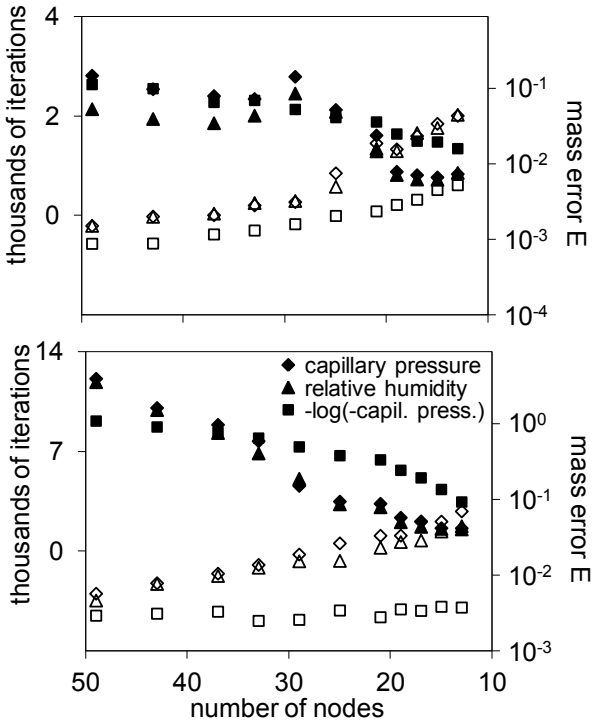

Figure 5: number of needed iterations and resulting mass errors for 'capillary absorption' for ceramic brick (top) and cement mortar (bottom). Full markers stand for the numbers of iterations (left axis), hollow markers represent the mass errors (right axis).

5. DISCUSSION OF RESULTS

5.1 Introductory observations

Some introductory observations are to be made first. Mostly, the mass error increases when the number of nodes decreases. The mass error can stem from three causes: convergence scheme errors, temporal discretisation errors and spatial discretisation errors. When repeating all simulations with a stricter convergence tolerance (Equation 5), which concurrently also reduces the length of the time steps (Equation 6), all mass errors remain comparable, thus indicating that spatial discretisation errors dominate the mass errors. The rising mass errors with decreasing number of nodes are thus logical, representing the effect of the coarsening discretisation.

Furthermore, in most cases, the number of iterations declines when the number of nodes drops. Such link has been observed in earlier publications (Kavetski et al., 2002; Janssen, 2010), but no straightforward explanation can be given here. This effect is probably a result of the complex interaction between spatial discretisation, temporal discretisation, convergence criteria and boundary conditions, all affecting the stability of the iteration process. The latter comment also applies to all further assessments of the numerical efficiency for the different potentials: while differences are observed, they are not always simple to explain in full. For that reason, the investigation reported here remains partly empirical.

5.2 Performance assessment

For hygroscopic adsorption, driving rain and isothermal drying, it can be noted that use of lp_c is most efficient: compared to p_c and φ, lp_c requires respectively around 60 % and 45 % less iterations. This increased efficiency often comes at a price in accuracy though: for most simulations, the mass error is biggest when using lp_c as moisture potential. As was stated earlier, the mass errors are dominated by spatial discretisation errors and the larger errors for lp_c should therefore not be attributed to the larger time steps that are common for these simulations. In some cases, the difference is minor, in other cases, it goes up to one order of magnitude or more. It should be noted though that the mass errors for hygroscopic adsorption, driving rain and isothermal drying do mostly remain limited to a few percent, which is negligible for many applications. For capillary absorption, on the other hand, the reverse observation is made: mass errors are now the smallest for lp_c, but its numerical efficiency is not superior to that of p_c and φ anymore. It should be noted again though that, except for the coarsest discretisations, the mass errors remain fairly small.

We are hence faced with contradictory observations. For hygroscopic adsorption, driving rain and isothermal drying, numerical efficiency is best for lp_c, medium for φ, and worst for p_c and numerical accuracy is best for p_c and φ and worst for lp_c. For capillary absorption, numerical accuracy is best for lp_c and worst for φ and p_c, while their numerical efficiencies are no longer much different.

5.3 Physical explanation

The distinction with relation to accuracy can likely be linked to different moisture potential magnitudes for hygroscopic adsorption, driving rain, isothermal drying versus capillary absorption. In the former, capillary pressures are mostly below the -10^5 Pa level (and the associated φ and lp_c levels), while in the latter the p_c-levels go up to -10^3 Pa. Capillary absorption thus leads to sharper moisture potential profiles compared to other three benchmarks, and the superior accuracy of lp_c shows that such are evidently more effortlessly represented with this particular 'smoothed' potential.

That difference in moisture potential magnitude may also bring about the distinction in relation to efficiency. Figure 6 depicts the moisture capacities and permeabilities for the cement mortar for the three potentials, see Equations 2a-c. In the -10^8 to -10^5 Pa range, the non-linearity is lowest for lp_c, medium for φ and largest for p_c. This is quantified via the ratio's of the largest over the smallest c- and k-values in the considered p_c-interval in Table 1. It is clear that the c- and k-variations are smallest for lp_c over φ over p_c, in the -10^8 to -10^5 Pa range. For the -10^8 to -10^3 Pa range, on the other hand, the c-ratio for lp_c raises with some four orders of magnitude, sharply inflating the non-linearity for lp_c. These relative non-linearities are evidently parallel to the relative efficiencies, within each benchmark and among different benchmarks.

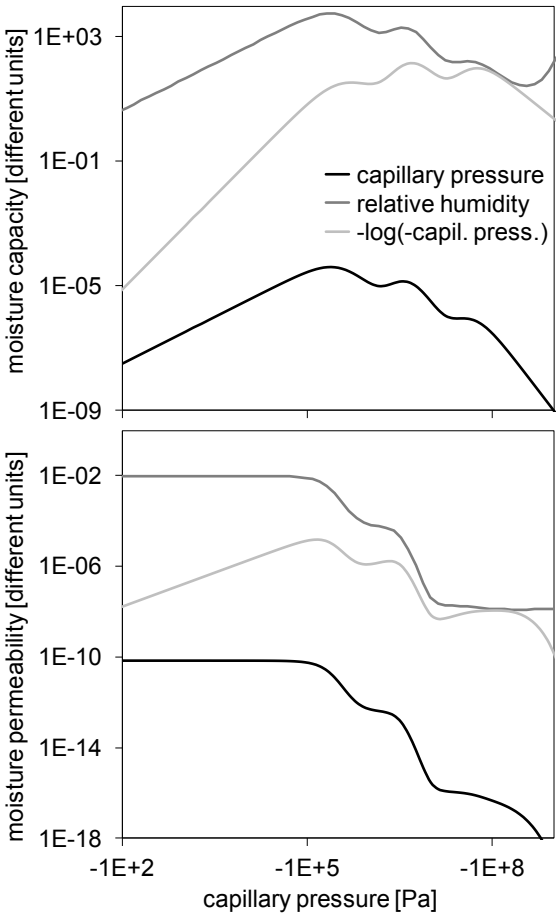

Figure 6: moisture capacities (top) and moisture permeabilities (bottom) for cement mortar, for the three considered potentials.

Table 1

Non-linearities of moisture capacity and permeability for cement mortar, for the three studied potentials, in the -10^8 to -10^5 Pa and -10^8 to -10^3 Pa ranges.

	-10^8 TO -10^5 Pa		**-10^8 TO -10^3 Pa**	
	c-ratio	**k-ratio**	**c-ratio**	**k-ratio**
p_c	$2.0 \cdot 10^2$	$1.5 \cdot 10^6$	$2.0 \cdot 10^2$	$1.8 \cdot 10^6$
φ	$8.1 \cdot 10^1$	$6.2 \cdot 10^5$	$1.5 \cdot 10^2$	$7.4 \cdot 10^5$
lp_c	$2.4 \cdot 10^1$	$3.1 \cdot 10^3$	$2.7 \cdot 10^5$	$3.1 \cdot 10^3$

For the hygroscopic adsorption, driving rain and isothermal drying benchmarks, lp_c requires the smallest number of iterations, followed first by φ and then by p_c. This order is in line with their relative non-linearities in the -10^8 to -10^5 Pa range, where these benchmarks operate. For capillary absorption, the efficiencies of φ and p_c are similar, equivalent to their non-linearities in the -10^8 to -10^3 Pa range. For lp_c, relative to φ or p_c, the non-linearity is bigger for c and smaller for k, rendering it more complex to judge. But it can cautiously be stated that the non-linearity of lp_c is similar to that of φ and p_c, being reflected in lp_c losing its edge over φ and p_c for capillary absorption.

5.4 Additional simulations

To further substantiate this parallel between efficiency and non-linearity, additional 'capillary absorption' simulations are performed for cement mortar. Therein -10^0, -10^2, -10^4 and -10^5 Pa are imposed as surface p_c, instead of the original -10^3 Pa (Equation 10). The outcomes – numbers of iterations & mass errors – of these additional simulations are very much similar to the original results, except for the number of required iterations for the lp_c potential. The latter are depicted in Figure 7. This figure deviates from the earlier versions: it only contains numbers of required iterations for the lp_c potential solely, and these are presented on a logarithmic scale. The cross markers are the original results, for $p_{c,s}$ equal to -10 Pa, as they appeared previously in Figure 5 (bottom).

For the two other potentials, p_c and φ, the numbers of required iterations do not change significantly when other $p_{c,s}$ values are imposed. Figure 6 does actually suggest that the non-linearity of the moisture capacity and permeability does not change much in the -10^8 to $-10^{5...1}$ Pa range for these two potentials. On the other hand, for lp_c the numbers of required iterations mount exponentially with the $p_{c,s}$ values, see Figure 7. Figure 6 does indeed indicate that the non-linearity of the moisture capacity increases dramatically when applying $p_{c,s}$ values closer to saturation. A detailed study of the numbers of required iterations moreover points out that the rising numbers of required iterations contain progressively more non-converging iteration sequences. This implies a deteriorating stability of the lp_c-based moisture transfer equation when closing in on saturation. These observations hence consolidate the previously established relation between efficiency and non-linearity.

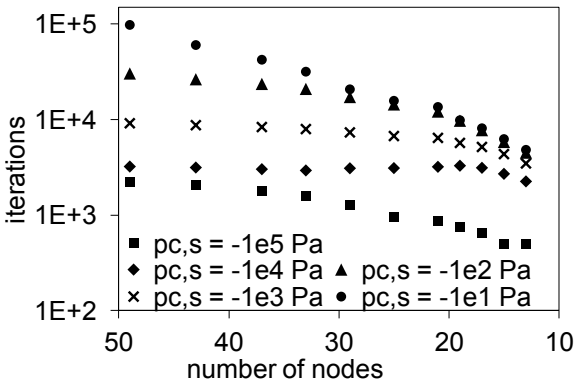

Figure 7: Numbers of required iterations for capillary absorption for cement mortar, based on lp_c, with different values for the surface p_c

5.5 Synthesis of findings

While sections 5.3 and 5.4 focused on cement mortar, it can be confirmed that similar conclusions arise for ceramic brick. The main difference is that, in the additional capillary absorption simulations, the model is no longer able to reach an acceptable solution for $p_{c,s}$ equal to -10^2 or -10^1 Pa, due to persistent instabilities.

In relation to numerical accuracy, the findings remain mixed. For the hygroscopic adsorption, driving rain, and isothermal drying benchmarks, lp_c performs a tad worse than φ and p_c, for the capillary absorption, the use of lp_c results in a significantly better accuracy. As the differences for the former three and the latter one are respectively negligible and non-negligible, it has to be concluded that use of lp_c can be recommended for accuracy purposes.

With respect to numerical efficiency, lp_c outperforms φ and p_c in the hygroscopic adsorption, driving rain, and isothermal drying benchmarks, whereas lp_c arrives at similar performances as φ and p_c in the capillary absorption benchmark. The additional capillary absorption simulations do however show that the strong non-linearity of lp_c's moisture capacity near saturation forms a core threat to its efficiency. For cement mortar, the numbers of required iterations rose exponentially with the surface capillary pressure $p_{c,s}$, for ceramic brick acceptable solutions could no longer be reached. In normal simulations of moisture transfer in building materials, such near-saturation conditions cannot be avoided. So, whereas lp_c performs slightly better in drier conditions, its numerical disadvantage in near-saturation conditions is too big to ignore.

For that reason, φ and p_c remain as numerically most efficient moisture potentials, whereas use of lp_c cannot be recommended. And as φ and p_c are equivalent to water vapour pressure/fraction/content and water chemical potential respectively, these potentials can equally be considered as numerically efficient.

6. CONCLUSIONS

In relation to numerical simulation of moisture transfer in building materials, there is still much disparity on which moisture potential is best used with respect to numerical efficiency and accuracy. Various implicit claims are around: a certain potential is assumed to dampen the non-linearities of the moisture transfer equation, a specfic potential is preferred over others as it operates in a more limited range, ... amid others. Unfortunately, valid support for this claims is usually lacking. For that reason, this study has investigated that issue, to allow a more rational choice of moisture potentials in current and future numerical tools.

The study has demonstrated that most potentials actually perform quite similarly, except for -log(-capillary pressure). The latter suffers from the strong non-linearity of the moisture capacity near saturation, and should for that reason be avoided in general moisture simulation tools. To conclude, it has to be noted that our numerical model uses the finite-element-spatial-discretisation approach, which may have some effect on the resulting findings. Currently however, use of pre-implemented partial differential equation solvers is on the rise (Van Schijndel, 2003, Tariku et al. 2010, Piaia et al., 2013), which primarily employ finite elements. For other models, this study at least puts forward an assessment methodology that can analoguously be applied.

REFERENCES

American Association of State Highway and Transportation Officials (AASHO), 2008. Bridging the gap: restoring and rebuilding the nation's bridges, Washington DC, United States.

Delgado J.M.P.Q., Barreira E., Ramos N.M.M., de Freitas V.P., 2013. Hygrothermal numerical simulation tools applied to building physics, Springer-Verlag Berlin and Heidelberg, Germany.

EN 15026, 2007. Hygrothermal performance of building components and building elements – Assessment of moisture transfer by numerical simulation.

Funk M., Wakili K.G., 2008. Driving potentials of heat and mass transport in porous building materials: a comparison between general linear, thermodynamic and micromechanical derivation schemes, Transport Porous Media 72: 273-294.

Hagentoft C.-E., Kalagasidis A.S., Adl-Zarrabi B., Roels S., Carmeliet J., Hens H., Grunewald J., Funk M., Becker R., Shamir D., Adan O., Brocken H., Kumaran K., Djebbar R., 2004. Assessment method of numerical prediction models for combined heat, air and moisture transfer in building components: benchmarks for one-dimensional cases, Journal of Thermal Envelope and Building Science, 27: 327-352.

Janssen H., Blocken B., Carmeliet J., 2007. Conservative modelling of the moisture and heat transfer in building components under atmospheric excitation, International Journal of Heat and Mass Transfer, 50: 1128-1140.

Janssen H., 2010. Adaptive Kronrod-Patterson integration of non-linear finite-element matrices, International Journal for Numerical Methods in Engineering, 81: 1455-1474.

Janssen H., 2011. Thermal diffusion of water vapour in porous materials: fact or fiction ? International Journal of Heat and Mass Transfer, 54: 1548-1562.

Janssens A., 2001. Advanced numerical models for hygrothermal research: 2DHAV model description, in 'Moisture analysis and condensation control' (editor: H.R. Trechsel). ASTM Manual 40. American Society for Testing and Materials, West Conshohocken, Pennsylvania, United States, 177-178.

Kavetski D., Binning P., Sloan S.W., 2002. Adaptive backward Euler time stepping with truncation error control for numerical modelling of unsaturated fluid flow. International Journal for Numerical Methods in Engineering, 53: 1301-1322.

Matsumoto M., Tanaka Y., 1991. A numerical analysis of moisture behavior in a porous wall by quasilinearized equations, Energy and Buildings, 16: 861-874.

Mendes N., Philippi P.C., Lamberts R., 2002. A new mathematical method to solve highly coupled equations of heat and mass transfer in porous media, International Journal of Heat and Mass Transfer, 45: 509-518.

Mudarri D., Fisk W.J., 2007. Public health and economic impact of dampness and mold, Indoor Air, 17: 226-235.

Piaia J.C.Z., Cheriaf M., Rocha J.C., Mustelier N.L., 2013. Measurements of water penetration and leakage in masonry wall: Experimental results and numerical simulation, Building and Environment, 61: 18-26.

Pedersen C.R., 1992. Prediction of moisture transfer in building constructions, Building and Evironment, 27: 387-397.

Qin M., Belarbi R., Aït-Mokhtar A., Nilsson L.-O., 2009. Coupled heat and moisture transfer in multi-layer building materials, Construction and Building Materials, 23: 967-975.

Steeman H.-J., Van Belleghem M., Janssens A., De Paepe M., 2009. Coupled simulation of heat and moisture transport in air and porous materials for the assessment of moisture related damage, Building and Environment, 44: 2176-2184.

Tariku F., Kumaran K., Fazio P., 2010. Transient model for coupled heat, air and moisture transfer through multilayered porous media, International Journal of Heat and Mass Transfer, 53: 3035-3044.

Van Schijndel A.W.M., 2003. Modeling and solving building physics problems with FemLab, Building and Environment, 38: 319-327.

Woloszyn M., Rode C., 2008. Tools for performance simulation of heat, air and moisture conditions of whole buildings, Building Simulation, 1: 5-24.